PAPER

Tailoring the bending pattern of non-uniformly flexible pitching hydrofoils enhances propulsive efficiency

To cite this article: Tianjun Han *et al* 2022 *Bioinspir. Biomim.* **17** 065003

Bioinspiration & Biomimetics

PAPER

Tailoring the bending pattern of non-uniformly flexible pitching hydrofoils enhances propulsive efficiency

Tianjun Han[1,*], Amin Mivehchi[1], Melike Kurt[2] and Keith W Moored[1]

[1] Mechanical Engineering and Mechanics, Lehigh University, Bethlehem, PA 18015, United States of America
[2] Aerodynamics and Flight Mechanics Group, Engineering and Physical Sciences, University of Southampton, Southampton SO17 1BJ, United Kingdom
* Author to whom any correspondence should be addressed.

E-mail: tih216@lehigh.edu

RECEIVED
17 March 2022

REVISED
17 June 2022

ACCEPTED FOR PUBLICATION
7 July 2022

PUBLISHED
7 September 2022

Keywords: bio-inspired propulsion, swimming/flying, non-uniformly flexible hydrofoil

Abstract

We present new measurements of non-uniformly flexible pitching foils fabricated with a rigid leading section joined to a flexible trailing section. This construction enables us to vary the bending pattern and resonance condition of the foils independently. A novel effective flexibility, defined as the ratio of added mass forces to elastic forces, is proposed and shown to provide a scaling for the natural frequencies of the fluid-structural system. Foils with very flexible trailing sections of $EI < 1.81 \times 10^{-5}$ N m^2 do not show a detectable resonance and are classified as 'non-resonating' as opposed to 'resonating' foils. Moreover, the non-resonating foils exhibit a novel bending pattern where the foil has a discontinuous hinge-like deflection instead of the smooth beam-like deflection of the resonating foils. Performance measurements reveal that both resonating and non-resonating foils can achieve high propulsive efficiencies of around 50% or more. It is discovered that non-uniformly flexible foils outperform their rigid and uniformly flexible counterparts, and that there is an optimal flexion ratio from $0.4 \leqslant \lambda \leqslant 0.7$ that maximizes the efficiency. Furthermore, this optimal range coincides with the flexion ratios observed in nature. Performance is also compared under the same dimensionless flexural rigidity, R^*, which highlights that at the same flexion ratio more flexible foils achieve higher peak efficiencies. Overall, to achieve high propulsive efficiency non-uniformly flexible hydrofoils should (1) oscillate above their first natural frequency, (2) have a flexion ratio in the range of $0.4 \leqslant \lambda \leqslant 0.7$ and (3) have a small dimensionless rigidity at their optimal flexion ratio. Scaling laws for rigid pitching foils are found to be valid for non-uniformly flexible foils as long as the measured amplitude response is used and the deflection angle of the trailing section β is $< 45°$. This work provides guidance for the development of high-performance underwater vehicles using simple purely pitching bio-inspired propulsive drives.

1. Introduction

A defining feature of swimming and flying animals is their use of flexible fins and wings [1–3]. In fact, with the right amount of flexibility, propulsive surfaces exhibit enhanced thrust, speed and efficiency over their rigid counterparts [4–15]. These conclusions are drawn from a considerable body of literature that has studied uniformly flexible foils, i.e. foils with uniform flexural rigidity, EI, across their chord and span, where E is the elastic modulus and I is the area moment of inertia. It has further been appreciated that the propulsive efficiency of uniformly flexible foils is maximized when the actuation frequency is at or near a natural frequency of the fluid-structural system [13, 14, 16–20] as long as the added mass forces acting on a foil dominate over its inertial forces, such as during underwater locomotion. However, the propulsive surfaces of animals are known to be *non-uniformly flexible*, where their flexural rigidity decreases from the leading edge to the trailing edge or from the center to the edge [21–24]. This observation has prompted recent studies to examine whether the basic principles of uniformly flexible foils extend to non-uniformly flexible foils.

Recent theoretical work has established that non-uniformly flexible foils can outperform uniformly flexible foils while echoing their basic principles, at

least within the assumptions of linear theory (small amplitudes of motion, non-deforming wakes and attached flow). Moore [25] showed that foils with non-uniform flexibility produced more thrust than uniformly flexible foils and that operating at resonance maximized the thrust. Floryan and Rowley [26] found that hydrofoils maximize their thrust at resonance, and if this was not possible then foils with a stiff leading edge (rather than uniform flexibility) would maximize their thrust. In their inviscid theory, efficiency did not peak at resonance; however, when drag was introduced efficiency peaks did emerge at the natural frequencies [27] as observed in experimental studies [13, 14, 19]. The importance of resonance in linear theory was found to extend to finite-amplitude motions, although nonlinear mechanisms distort performance peaks making them occur in the vicinity of resonance rather than always coincident [20].

The primary difference between non-uniformly flexible foils and their uniform counterparts is in their bending pattern, which can be tailored through variations in the thickness and/or elastic properties along their characteristic dimensions [21, 28–31]. Yeh *et al* [29] showed that the bending pattern of foils with tapered thickness maintained a large trailing-edge amplitude over a wide range of actuation frequencies, not just at resonance. This led to superior thrust and efficiency/economy performance compared with uniformly thick foils. David *et al* [32] constructed rigid foils with flexible trailing-edge flaps of varying lengths. These foils had characteristically different bending patterns; however, their first natural frequency varied widely for each foil leading to performance comparisons at vastly different frequencies relative to resonance. Zeyghami and Moored [31] adopted a non-uniformly flexible foil model in two-dimensional inviscid simulations by placing a torsional spring at different locations along the chord to vary the bending pattern and resonance condition independently. They determined that both the flexibility and the bending pattern played a large role in maximizing the thrust and efficiency of pitching foils. The propulsive surfaces of animals even exhibit the same bending pattern across species, with a flexion point occurring at around two-thirds of the length of a propulsor [33] despite their wide range of propulsive structures and material properties (e.g. bone, muscle, skin membrane and feathers).

These studies highlight the importance of both resonance and the bending pattern in maximizing the performance of non-uniformly flexible foils. To date, no finite-amplitude, viscous flow studies have comprehensively varied the bending pattern of foils while comparing their performance below, at and above the first natural frequency. To address this unresolved issue we construct foils composed of a rigid leading section with a flexible trailing section, of constant flexural rigidity, joined at the flexion point. In this way, non-uniformly flexible foils are formed with a simple chordwise step function in their flexural rigidity going from an infinite to a finite value along the chord. Importantly, the bending pattern can be altered independently from the first natural frequency by varying (1) the flexion ratio $\lambda = c_r/c$ where c_r is the chord length of the rigid section and c is the total chord length and (2) the flexural rigidity of the trailing section.

We advance our understanding of non-uniformly flexible foils by disentangling the effect of the bending pattern from the resonance condition to discover that there is an optimal flexion ratio of $0.4 \leqslant \lambda \leqslant 0.7$, in line with flexion ratios observed in nature [33], where non-uniformly flexible foils can outperform their rigid and uniformly flexible counterparts achieving efficiencies greater than 50% for purely pitching motions. The paper is organized in the following manner. Section 2 describes the non-uniformly flexible foils as well as the experimental setup and methods employed. Section 3 presents a new definition of the effective flexibility derived from the Euler–Bernoulli beam equation that is valid for both uniformly flexible and non-uniformly flexible foils. This represents a generalization of the scaling law for the fluid-structural natural frequencies presented in Quinn *et al* [14]. Section 4 presents propulsive performance results. Section 5 shows the effect of varying the bending pattern under the same dimensionless flexural rigidity. Section 6 describes scaling law analysis, and section 7 summarizes the conclusions of the paper.

2. Experimental methods

We examined hydrofoils of a rectangular planform shape with an aspect ratio $AR = s/c = 2$, where the span and chord lengths are $s = 0.19$ m and $c = 0.095$ m, respectively (figure 1). The hydrofoils are composed of a rigid leading section (carbon fiber sheet, thickness 0.8 mm) and a flexible trailing section (polyester shim stock of varying thicknesses) with a NACA 0018 coupler (chord length 25 mm, but truncated at two-thirds of the chord) attached to the leading edge for streamlining. This construction produces a chordwise non-uniform flexibility distribution that is represented as a simple step function from an effectively infinite to a finite flexural rigidity. As stated in the introduction, the flexion ratio is defined as the ratio of the length of the rigid section to the entire chord length of the foil, $\lambda = c_r/c$. Note that the rigid section length refers to the combined length of the carbon fiber sheet and the leading edge coupler. If $\lambda = 1$, a foil is fully rigid. If $\lambda \to 0$, a foil is uniformly flexible ($\lambda = 0.1$ in the current study). Otherwise, a foil is non-uniformly flexible and a variation in the flexion ratio will vary the bending pattern of the foil. This non-uniformly flexible foil construction enables

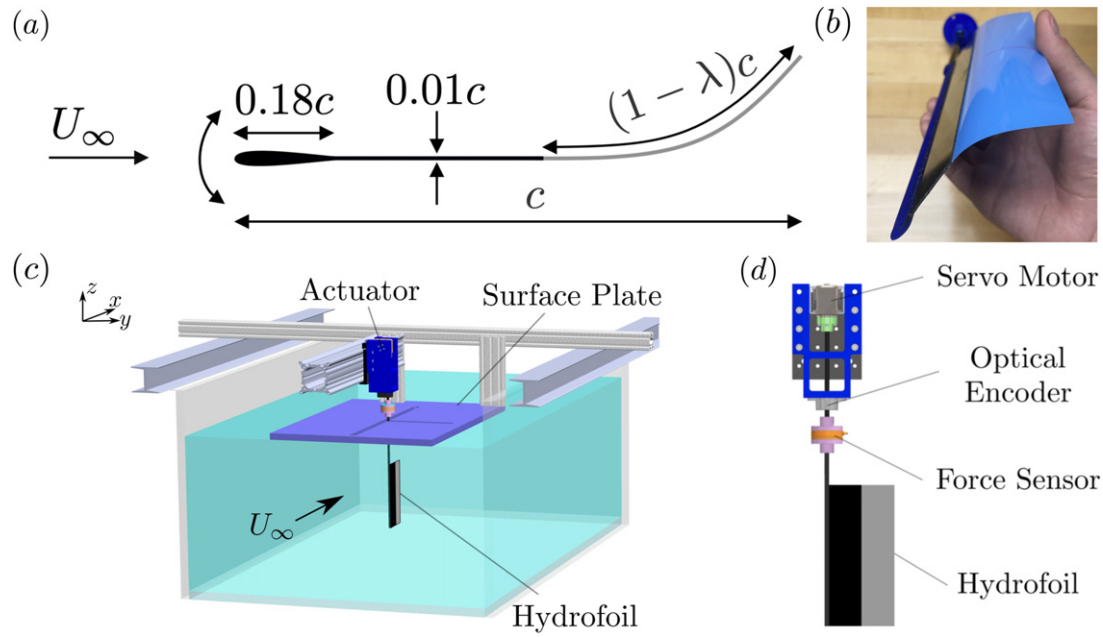

Figure 1. (a) Schematic of a non-uniformly flexible hydrofoil undergoing purely pitching motion with a flexion ratio of $\lambda = 0.5$. The black and gray portions depict the rigid leading section and the flexible trailing section, respectively, at a snapshot in time. (b) Photograph of a non-uniformly flexible foil. (c) Schematic of the water channel facility and experimental setup. (d) Detailed view of the pitching actuation mechanism.

the independent variation in the bending pattern and the flexural rigidity of the flexible portion.

Experiments were conducted in a free-surface, recirculating water channel with a test section of 4.9 m long, 0.93 m wide and 0.61 m deep. A sequence of honeycomb meshes and screens are arranged upstream of the test section to attain uniform flow and a turbulence intensity of less than 0.3%. The freestream velocity $U_\infty = 0.094$ m s^{-1} was maintained throughout experiments to achieve a chord-based Reynolds number $Re_c = U_\infty c/\nu = 9000$, where ν is the kinematic viscosity of the water. Figure 1 depicts the experimental apparatus in the water channel facility. An acrylic surface plate was used to reduce surface waves and had a width of 0.35 m with lengths of 0.6 m and 0.5 m downstream and upstream, respectively, of the leading edge of the foil.

The hydrofoil was driven in a sinusoidal pitching motion about the leading edge, $\theta(t) = \theta_0 \sin(2\pi ft)$, by a servo motor (Dynamixel MX-64T), where θ_0 is the pitching amplitude, f is the frequency and t is time. The pitching amplitude was set to $\theta_0 = 8.6°$, leading to a peak-to-peak trailing edge amplitude of $A_0 = 2c\sin(\theta_0) = 0.3c$ for the fully rigid foil. The instantaneous pitching angle was measured with an incremental encoder (US digital E5 optical encoder) and observed to deviate from the input waveform by less than 1.7%. Additionally, angular position measurements were used with a second-order central difference scheme to calculate the instantaneous angular velocity, $\dot{\theta}$, used in the power input measurements described below. Because the motion of the flexible trailing section depends upon the fluid loading, the bending pattern and peak-to-peak trailing-edge amplitude, A, were measured with a camera (GoPro Hero 7) capturing the mid-span motion illuminated by a continuous laser sheet. The peak-to-peak trailing-edge amplitude was then measured with motion-tracking software and it showed a cycle-to-cycle variation of less than 2%. To effectively resolve the amplitude peaks at resonance, the frequency was varied over the range 0.15 Hz $\leqslant f \leqslant$ 2.0 Hz in 0.05 Hz increments for the motion-tracking analysis. For propulsive performance measurements, the frequency was varied over a coarser range of 0.4 Hz $\leqslant f \leqslant$ 2.0 Hz with an increment of 0.1 Hz.

The pitching actuation mechanism (see figure 1(d)) was composed of a hydrofoil connected to a servo motor by a carbon fiber drive rod with an in-line optical encoder and a six-axis force/torque sensor (ATI Nano43). The force/torque sensor measured the net thrust force, T, and pitching moment, M_θ, acting on the foil. The instantaneous power input to the foil was then calculated as $P = M_\theta\dot{\theta}$, which was determined by subtracting the power input in air from the power input in water to eliminate the inertial power input and isolate the power input to the fluid. The thrust and power were then time-averaged over 60 pitching cycles during each trial. The mean values over five trials of the time-averaged thrust, $\overline{T}$, and power, $\overline{P}$, are reported as the dynamic pressure-based thrust and power coefficients, respectively

$$C_T = \frac{\overline{T}}{\frac{1}{2}\rho {U_\infty}^2 cs} \quad \text{and} \quad C_P = \frac{\overline{P}}{\frac{1}{2}\rho {U_\infty}^3 cs}. \tag{1}$$

Here, ρ is the density of the fluid. The propulsive efficiency is defined as

$$\eta = \frac{C_T}{C_P} = \frac{\overline{T} U_\infty}{\overline{P}}. \tag{2}$$

The measurement uncertainties are less than $\varepsilon_{C_T} = \pm 0.015$, $\varepsilon_{C_P} = \pm 0.0034$ and $\varepsilon_\eta = \pm 4\%$ across the entire testing domain.

3. Hydrofoil elastic response

The small deflections, h, of the flexible trailing section can be modeled with the Euler–Bernoulli beam equation [14, 34]

$$\rho_m s\delta \frac{\partial^2 h}{\partial t^2} + EI\frac{\partial^4 h}{\partial x^4} = \mathscr{F}_{\text{ext}} \tag{3}$$

where ρ_m and δ are the material density and thickness, respectively, of the flexible trailing section, x is the chordwise position along the trailing section and $\mathscr{F}_{\text{ext}}$ are the external fluid forces acting on the trailing section. The added mass force can be extracted from $\mathscr{F}_{\text{ext}}$ and written on the left-hand side as a characteristic added mass per unit length for the trailing section, $\rho s(1-\lambda)c$, times the acceleration, $\partial^2 h/\partial t^2$. As noted in [14] for underwater propulsion, $\rho_m/\rho = \mathscr{O}(1)$ and $\delta \ll (1-\lambda)c$ (except when $\lambda \to 1$ in which case the hydrofoil is effectively fully rigid). This leads to the material's inertia being negligible compared with its added mass. Applying this simplification, the Euler–Bernoulli equation can be rewritten in a dimensionless form as

$$\Pi_k^2 \frac{\partial^2 H^*}{\partial T^{*2}} + \frac{\partial^4 H^*}{\partial X^{*4}} = \mathcal{F}^*_{\text{ext}} \tag{4}$$

where $H^* = h/A$, $T^* = tf$, $X^* = x/[(1-\lambda)c]$ and $\mathcal{F}^*_{\text{ext}} = \mathcal{F}'_{\text{ext}}(1-\lambda)^4 c^4/EIA$, with $\mathcal{F}'_{\text{ext}}$ being the external fluid force per unit length without the added mass force acting on the trailing section. The effective flexibility

$$\Pi_k = (1-\lambda)^{\frac{5}{2}}\sqrt{\frac{\rho s f^2 c^5}{EI}}, \tag{5}$$

represents the ratio of the added mass forces to the elastic forces and it is a generalization of that presented in Quinn *et al* [14] and the continuously flexible equivalent of the discrete torsional-spring-based effective flexibility presented in Zeyghami and Moored [31]. The homogeneous form of equation (4) can be solved exactly to determine that the ratio of the driving frequency to the fluid-structural natural frequencies (when only added mass fluid forces are considered) is directly proportional to the effective flexibility as $f/\hat{f}_i = \Pi_k \lambda_i^2$, where $\hat{f}_i$ and λ_i are the ith natural frequency and associated eigenvalue, respectively. Hence this highlights the importance of the effective flexibility in defining the elastic response of the hydrofoils.

Fourteen foils of varying flexion ratio and trailing section flexural rigidity, including one fully rigid foil, were tested. Table 1 shows a diagonal band of foil properties, which were chosen such that all foils were pitched at frequencies below, at and above their first fluid-structural natural frequency given the range of testing frequencies defined in section 2. This led to more flexible trailing sections with their decreasing length (increase in the flexion ratio); hence the diagonal structure to the testing matrix. The non-uniformly flexible foils are labeled $F_2 - F_{13}$ while the rigid foil is F_∞. Note that F_1 is considered to be uniformly flexible in the current study.

Figure 2 presents the normalized peak-to-peak trailing edge amplitudes of the flexible foils as a function of the effective flexibility. For all the foils, the spanwise deflection of the trailing edge was found to be negligible. If $A/A_0 > 1$ the flexible foils experience an amplitude amplification compared with the rigid foil, while for $A/A_0 < 1$ there is an amplitude reduction. The resonance condition is considered to be the location where A/A_0 is locally maximized. As expected, foils $F_1 - F_9$ show clear resonances, and their amplitude peaks all collapse to the same value of $\Pi_k = 0.86$. This shows that the proposed effective flexibility provides an accurate scaling of the resonance condition for foils with uniform as well as non-uniform flexibility. Additionally, their maximum A/A_0 is around 1.2–1.3, which agrees well with the work of Dai *et al* [11] and Dewey *et al* [13]. However, for foils $F_{10} - F_{13}$ whose trailing section flexural rigidity is $EI < 1.81 \times 10^{-5}$ N m^2, there is no clear resonance and their amplitude remains amplified for the entire range of effective flexibility examined (figure 2(b)). In fact, their A/A_0 can exceed that of the foils exhibiting a clear resonance with values up to 1.7.

To characterize not just the trailing edge amplitude response but also the bending patterns of the hydrofoils, snapshots of the foils at 12 equally spaced phases in one oscillation period are superimposed (figure 3). Here we choose foils F_1 and F_6 (with a resonance condition), as well as foil F_{10} (without a resonance condition) to illustrate the bending patterns. Regardless of the flexion ratio, foils F_1 and F_6 show a smooth curvature all along the foil at and above resonance like that observed in uniformly flexible foils [14]. However, the bending pattern of foil F_{10} shows a discontinuity in the slope of the surface at the flexion point. In fact, the flexible section retains a constant slope along its length at any instantaneous time and, in this way, behaves like a flexible hinge similar to that examined numerically [31] and theoretically

Table 1. Material and structural properties of the hydrofoils. Note that the flexural rigidity of the rigid foil is considered to be effectively infinite since it shows negligible deformation during experiments.

EI (N m^2)	$\lambda = 0.1$	$\lambda = 0.2$	$\lambda = 0.3$	$\lambda = 0.4$	$\lambda = 0.5$	$\lambda = 0.6$	$\lambda = 0.7$	$\lambda = 0.8$	$\lambda = 1$
2.83×10^{-4}	F_1	F_2	F_3						
8.39×10^{-5}			F_4	F_5					
4.39×10^{-5}				F_6	F_7				
1.81×10^{-5}					F_8	F_9			
2.26×10^{-6}						F_{10}	F_{11}		
6.71×10^{-7}							F_{12}	F_{13}	
∞									F_∞

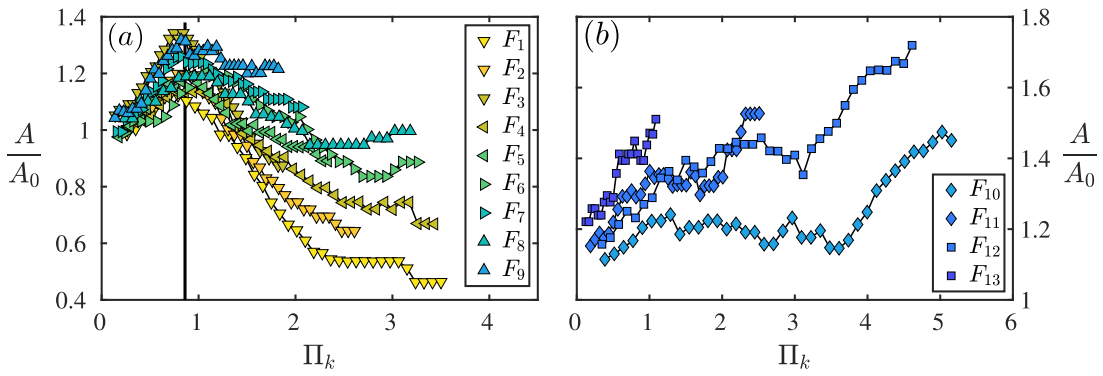

Figure 2. Normalized peak-to-peak trailing-edge amplitude as a function of the effective flexibility. (a) Foils showing a resonance condition and (b) foils without a detectable resonance condition. The marker styles are mapped to the flexural rigidity of the trailing section while the marker colors, from light yellow to dark blue, correspond to the flexion ratios from 0.1 to 0.8, respectively.

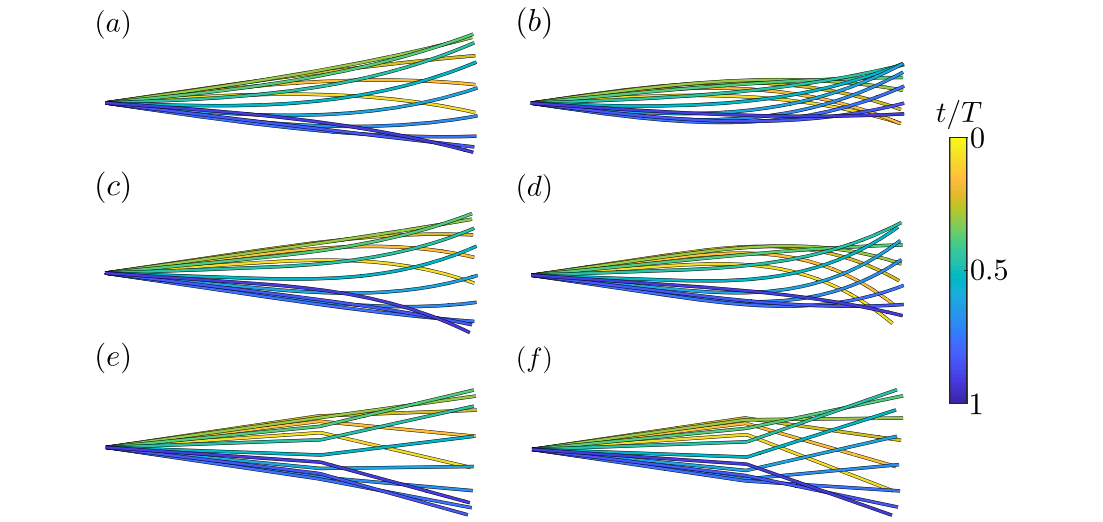

Figure 3. Bending patterns of foils F_1, F_6 and F_{10}, which have flexion ratios of $\lambda = 0.1$, 0.4 and 0.6, respectively. Foils (a)F_1, (c)F_6 and (e)F_{10} operating at the predicted first natural frequency with $\Pi_k = 0.86$. Foils (b)F_1, (d)F_6 and (f)F_{10} operating above the predicted first natural frequency with $\Pi_k = 2$.

[35, 36]. When all three foils are driven at their predicted first natural frequencies ($\Pi_k = 0.86$; although foil F_{10} does not show a resonance condition) their amplitude envelopes monotonically increase along the chord [11, 37] and their mode shapes are characteristic of a first bending mode [14, 19]. Above their predicted first natural frequency, the foils show a mode shape transitioning towards a second bending mode [14, 19].

4. Propulsive performance of non-uniformly flexible foils

Force and power measurements were conducted to identify the role of the bending pattern in driving the propulsive performance of non-uniformly flexible hydrofoils. Throughout this section the hydrofoils that exhibit a resonance condition and have a beam-like smooth deformation, described as 'resonating'

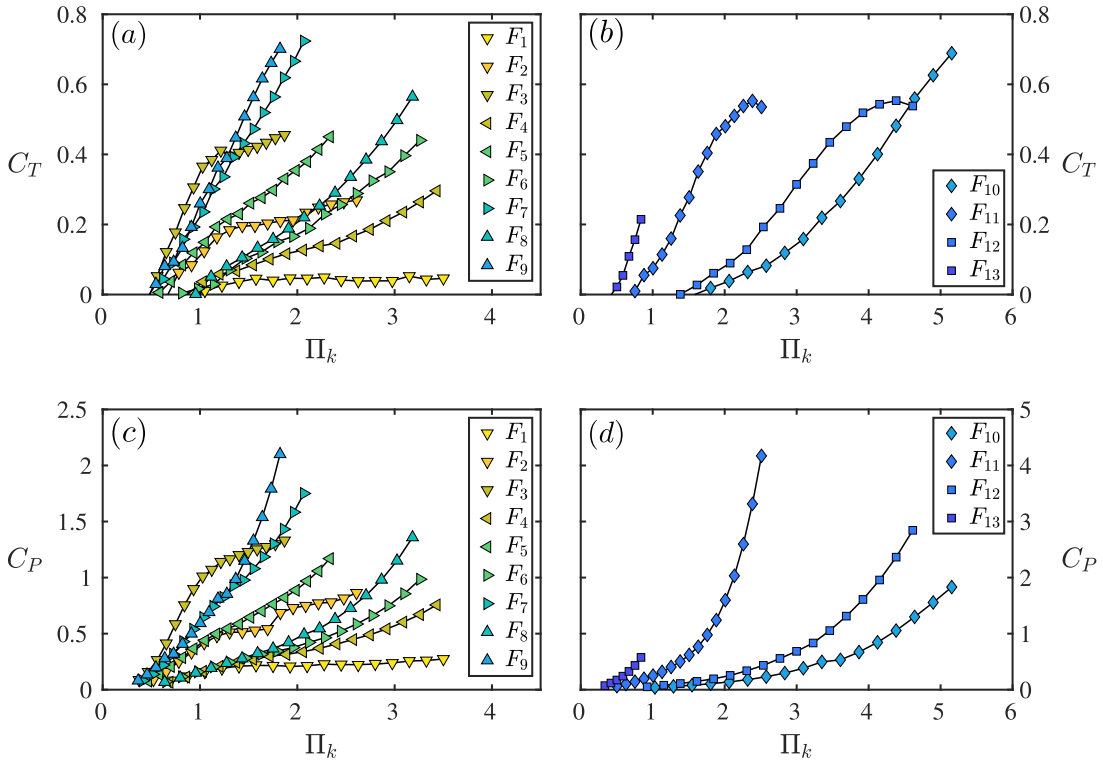

Figure 4. Propulsive performance as a function of effective flexibility. Thrust coefficient for (a) the resonating foils and (b) the non-resonating foils. Power coefficient for (c) the resonating foils and (d) the non-resonating foils.

foils, will be separated from those that do not show a resonance condition and have a hinge-like discontinuous deformation, described as 'non-resonating' foils.

Figures 4(a) and (b) present the thrust coefficient as a function of the effective flexibility. For all the foils there is a monotonic increase in thrust with an increase in effective flexibility. However, the thrust trends of the resonating and non-resonating foils are characteristically different. The resonating foils show a near linear increase in thrust at sufficiently low effective flexibility of $\Pi_k \lesssim 1$, then a decrease in the slope of the thrust curve at or just above resonance in the range $1 \lesssim \Pi_k \lesssim 2$, followed by an increase in slope of the thrust curve for greater effective flexibility of $\Pi_k \gtrsim 2$ as seen previously [13, 14]. Also, with the proper definition of Π_k the drag-to-thrust transition occurs in the narrow range $0.5 \leqslant \Pi_k \leqslant 1$. In contrast, the non-resonating foils show a wider range for the drag-to-thrust transition $0.5 \leqslant \Pi_k \leqslant 2$, and a decrease in the slope of the thrust curves happens above, and in some cases well above, the predicted first natural frequency in the range $1.5 \leqslant \Pi_k \leqslant 5$. This highlights the dissociation of these foils from resonance.

All the foils exhibit clear trends with variations in the flexural rigidity and the flexion ratio. When the flexural rigidity is held constant and the flexion ratio increases, such as among foils F_1, F_2 and F_3, the thrust production increases at the same effective flexibility. This is intuitively expected since with an increasing flexion ratio there is an increasing large rigid portion of the foils, and more rigid foils tend to generate larger thrust coefficients, at least at sufficiently high driving frequencies [10, 13, 28, 30]. When the flexion ratio is held constant and the flexural rigidity *decreases*, such as between foils F_{11} and F_{12}, there is a subsequent decrease in the thrust production at the same effective flexibility. Again, this occurs since the overall flexibility of the foil decreases as the trailing section becomes more flexible.

The power coefficient is presented in figures 4(c) and (d) as a function of the effective flexibility. Like the thrust, the power coefficient exhibits a monotonic trend with increasing effective flexibility. For the resonating foils, the trend in the power coefficient follows closely with its trend in thrust, where there is a decrease in the slope of the curve around resonance and an increase in the slope at higher effective flexibility. Surprisingly, for the non-resonating cases, the power coefficient *does not* show a decrease in the slope like the resonating foils, and, in fact, has an ever-increasing slope with increasing flexibility, reminiscent of rigid pitching foils [13, 38]. For both resonating and non-resonating foils, if the flexural rigidity is held constant and the flexion ratio increases, and vice versa, the foils consume more power at the same effective flexibility, similar to the thrust.

Figure 5 presents the propulsive efficiency as a function of the effective flexibility. The resonating foils show a peak in efficiency in the range $1 \leqslant \Pi_k \leqslant 3$

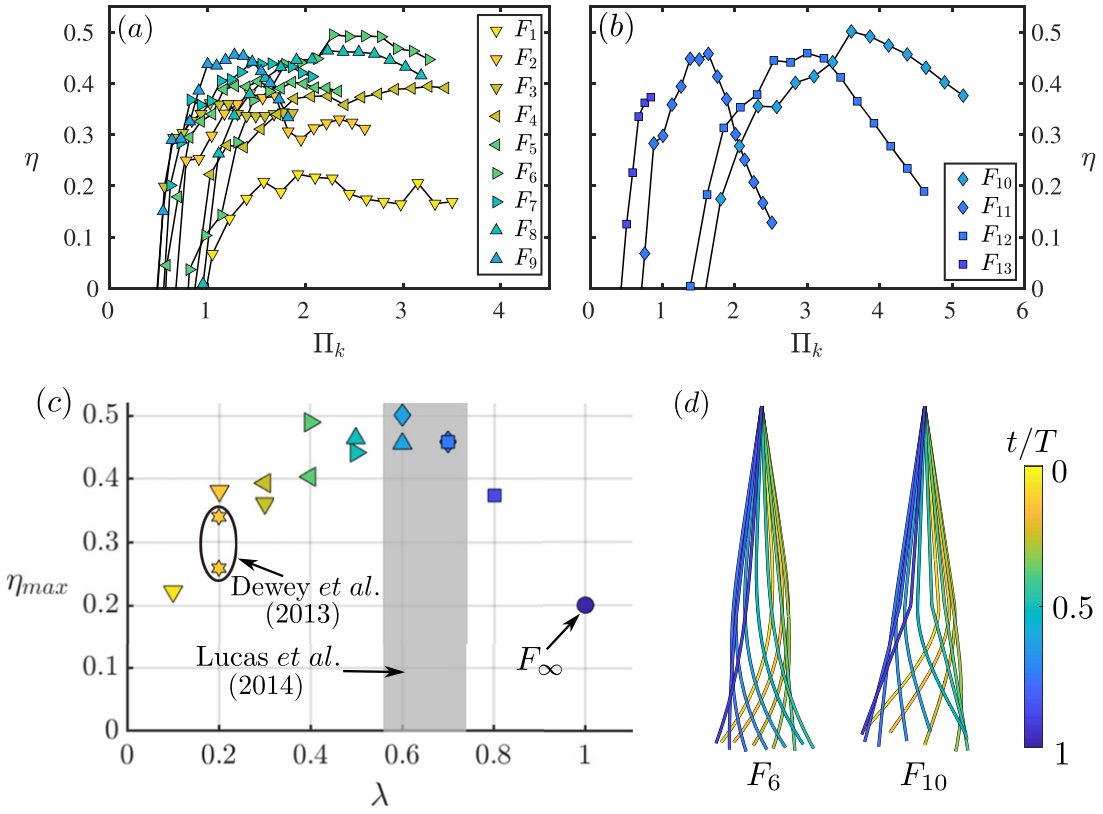

Figure 5. Propulsive efficiency as a function of Π_k for (a) resonating foils and (b) non-resonating foils. (c) Maximum propulsive efficiency of each foil extracted from (a) and (b) as a function of the flexion ratio. Maximum efficiency data for the $AR = 2$ foils in Dewey *et al* [13] as well as the rigid foil data are added for reference. The shaded area is the range of flexion ratio found in biological data as presented in Lucas *et al* [33]. (d) Bending patterns of F_6 and F_{10} at their the maximum efficiency operating conditions of $\Pi_k = 2.3$ and $\Pi_k = 3.6$, respectively.

with an extended range of high efficiency at higher effective flexibility, like that observed in Dewey *et al* [13], with the exception of foil F_9, which is on the cusp of behaving like a non-resonating foil. The non-resonating foils show a more well-defined efficiency peak with a sharp decline in efficiency at higher effective flexibility than that of the peak. These efficiency peaks are coincident with inflection points in the non-resonating foil thrust coefficient curves. Therefore, the sharp decline in efficiency is driven by a decline in the slope of the thrust curve above the efficiency peak paired with a continually increasing slope in the associated rigid-foil-like power curve.

The peak efficiency is extracted from both the resonating and non-resonating efficiency data and compiled in figure 5(c) as a function of the flexion ratio. For reference, the peak efficiencies for the $AR = 2$ foils (the same AR as the current study) from Dewey *et al* [13] and the rigid foil F_∞ are added. A clear optimal flexion ratio emerges in the range $0.4 \leqslant \lambda \leqslant 0.7$ where the efficiency is maximized above 45% with an efficiency greater than $\eta = 50\%$ at $\lambda = 0.6$. This highlights that the tailoring of the bending pattern of non-uniformly flexible foils, via variations in the flexion ratio, can significantly enhance their propulsive efficiency over either their rigid or uniformly flexible foil counterparts. Moreover, the optimal range of flexion ratios coincides with flexion ratios observed in nature (denoted by the shaded area in figure 5(c)) across a wide range of species [33]. This suggests that animals may have evolved bending patterns with flexion ratios around $\lambda = 0.6$ in order to enhance their propulsive efficiency.

It is surprising to see both resonating (F_6; $\lambda = 0.4$) and non-resonating (F_{10}; $\lambda = 0.6$) foils achieving equivalent peak efficiencies, within their uncertainty, with quite different bending patterns (figure 5(d)). At their peak efficiencies, foil F_6 exhibits a beam-like smooth deformation while foil F_{10} is showing transition from a hinge-like discontinuous deformation to a beam-like smooth deformation. Future work will focus on quantifying the flow structures around these foils, especially at the flexion point where flow separation at the sharp hinge of foil F_{10} would be expected.

5. Tailoring the bending pattern at the same dimensionless flexural rigidity

In order to further investigate the effect of tailoring the bending pattern, a dimensionless flexural rigidity is used:

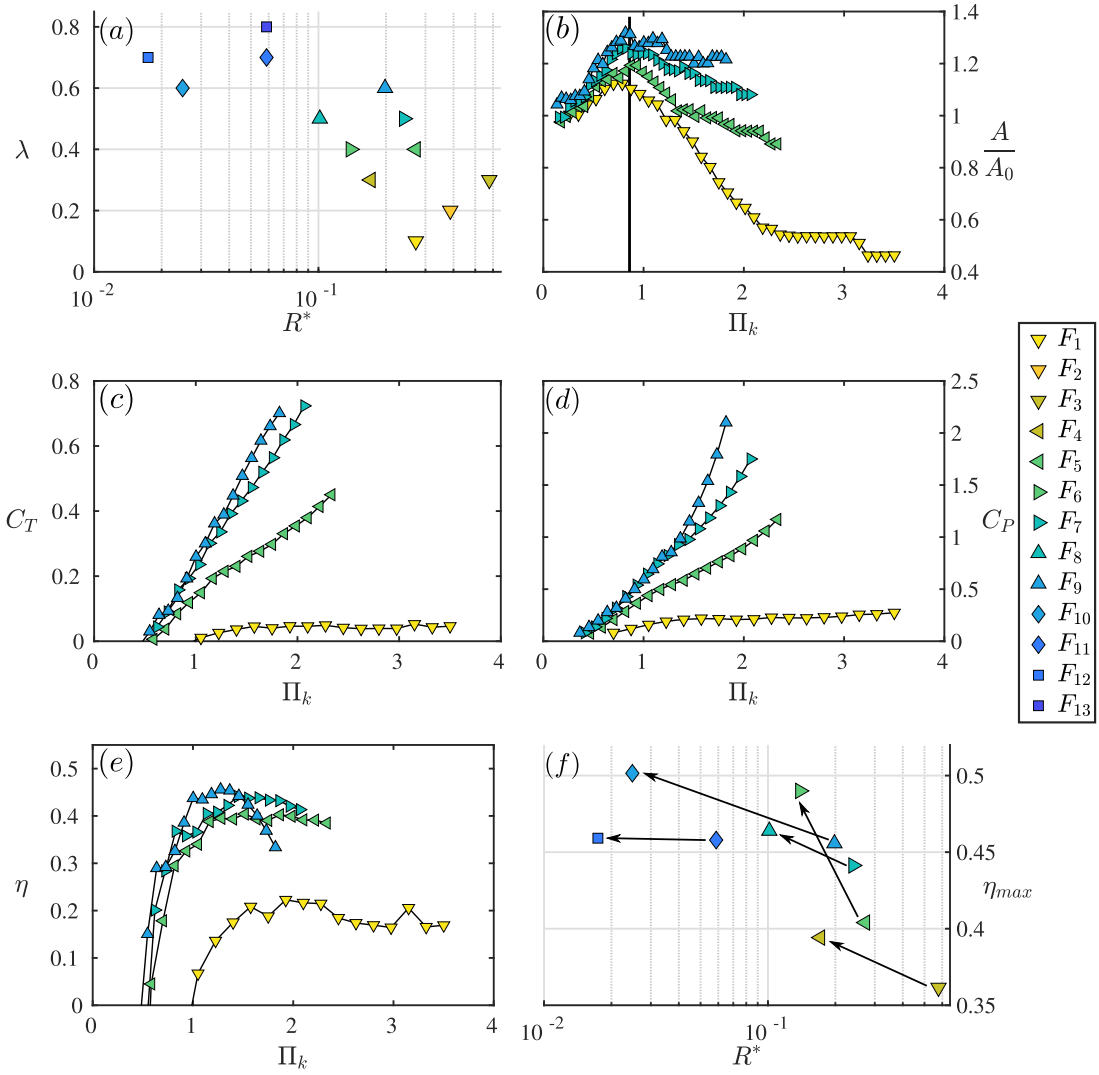

Figure 6. (a) Flexion ratio of all foils as a function of dimensionless rigidity. (b) Dimensionless amplitude, (c) thrust coefficient, (d) power coefficient and (e) efficiency for foils F_1, F_5, F_7 and F_9, which all have $R^* \simeq 0.24$. (f) Maximum propulsive efficiency of the foils that share a flexion ratio with another foil as a function of the dimensionless rigidity. Throughout this figure the colors are mapped to the flexion ratio as noted previously.

$$R^* = \frac{EI}{\rho U_\infty^2 sc^3(1-\lambda)^3.} \tag{6}$$

When this variable is conserved, the dimensionless displacement of the trailing section under a unit load is also conserved, thereby describing the effects of stiffness variations independent of the resonance condition [32]. Figure 6(a) presents the dimensionless rigidity of the foils mapped to their flexion ratio. Foils F_1, F_5, F_7 and F_9 have nearly the same dimensionless rigidity with values of $R^* = 0.27$, 0.27, 0.24 and 0.2, respectively, which are all around $R^* \simeq 0.24$. In figures 6(b)–(e) only these four foils are presented to highlight the effect of variations in flexion ratio at the same dimensionless rigidity. When the dimensionless rigidity is conserved and foils are oscillated at the same resonance condition (the same Π_k), then increasing the flexion ratio from 0.1 to 0.6 increases the peak-to-peak amplitude, thrust production and power consumption. As found in figure 5(c) a flexion ratio of $\lambda = 0.6$ generates the maximum propulsive efficiency, which highlights that the flexion ratio, and thus the bending pattern, is the main driver for maximizing the efficiency beyond operating above the first resonant frequency. However, by plotting only the maximum efficiencies from foils that share a flexion ratio with another foil (figure 6(f)) it can be observed that more flexible foils produce higher maximum propulsive efficiencies at the same flexion ratio (same color), at least within our data set. It is quite likely that further work could reveal an optimal dimensionless rigidity at each flexion ratio.

Now a framework for optimizing non-uniformly flexible foils can be postulated. Their efficiency can be maximized by: (1) oscillating them above their first natural frequency, (2) tuning their flexion ratio to $0.4 \leqslant \lambda \leqslant 0.7$ and (3) minimizing their dimensionless rigidity at the optimal flexion ratio.

6. Scaling law analysis

We postulate that previously developed scaling laws for purely pitching *rigid* foils [39] will capture the physics of non-uniformly flexible foils operating around their first natural frequency, as long as the *measured trailing edge amplitude response* is used in the scaling law calculations. In this way the effects of flexibility will be implicitly implemented into the scaling laws, and as such will not provide a predictive model using only variables and parameters known a priori. Still, these scaling laws will be informative as to whether the flow physics of non-uniformly flexible pitching foils are well-modeled in the rigid foil scaling laws. The previously developed scaling laws are a combination of the added mass and circulatory forces from classical linear theory [36] with additional nonlinear terms that are not accounted for in linear theory. Further details of their development and application, as well as more in-depth descriptions can be found in [39–42]. The thrust coefficient scaling law is the superposition of three terms

$$C_T = c_1\phi_1 + c_2\phi_2 + c_3\phi_3 \tag{7}$$

$$\text{with: } \phi_1 = St^2,$$

$$\phi_2 = St^2\left[(F^2+G^2)\left(\frac{1}{\pi^2k^2}+\frac{9}{4}\right) + \frac{G}{2\pi k} - \frac{3F}{2} - \frac{F}{\pi^2k^2}\right],$$

$$\phi_3 = St^2A^*,$$

where c_1, c_2 and c_3 are constants to be determined, F and G are the real and imaginary components of Theodorsen's lift deficiency function, respectively [35], the reduced frequency is $k = fc/U_\infty$ and the dimensionless trailing edge amplitude is $A^* = A/c$. The first and second terms are the added mass and circulatory thrust forces, respectively, from linear theory. The second term is included here for completeness; however, it plays a minor role scaling the performance of experimental data and can be neglected without a significant loss in accuracy in most cases. The third term is not accounted for in linear theory and corresponds to the form drag of the oscillating foil. The power coefficient scaling law is also the superposition of three terms

$$C_P = c_4\phi_4 + c_5\phi_5 + c_6\phi_6 \quad \text{with: } \phi_4 = St^2,$$

$$\phi_5 = \frac{St^4}{k}\left(\frac{k^*}{1+k^*}\right), \qquad \phi_6 = St^4k^*, \tag{8}$$

where c_4, c_5 and c_6 are constants to be determined and $k^* = k/(1+4St^2)$. The first term represents the added mass power from linear theory. The second and third terms are nonlinear corrections not present in linear theory that account for large-amplitude motions and the proximity of the trailing edge vortex to the foil, respectively. While these scaling laws are valid for nominally two-dimensional foils, the fully three-dimensional version [41] is not necessary since the aspect ratio of the foils is constant throughout this study. This leads to a difference in the fitted coefficients found with the current data compared with equivalent nominally two-dimensional foils; however, there should be no change in how well the data collapse.

Figure 7 presents the thrust and power data compared with the prediction of the scaling laws. Using *only the resonating foil data*, linear regression was performed by minimizing the squared residuals. It should be noted that the thrust scaling does not model the net thrust, but the pure thrust. Therefore, the profile drag coefficient of $C_{D,0} = D/(1/2\rho U_\infty^2 sc) = 0.04$, where D is the time-averaged drag of the static foils, was added to the reported thrust coefficients, linear regression was then performed on those data and finally the drag coefficient was subtracted from the thrust scaling law to arrive at a prediction of the net thrust. In this way, the coefficients were determined to be $c_1 = 1.39$, $c_2 = -4$, $c_3 = -1.52$, $c_4 = 4.68$, $c_5 = -16.16$ and $c_6 = 1.73$. If the data are accurately predicted by the scaling laws then they will collapse to the solid reference line of slope 1 shown in the figure. Indeed, figures 7(a) and (c) show a good collapse of the resonating foil data from foil F_1 to foil F_9. This shows that if a scaling law for the trailing edge amplitude response were determined as a function of the input kinematic variables, and the structural and material properties, then the scaling laws would accurately capture the *overarching* flow physics of non-uniformly flexible foils. However, even with using the measured trailing edge amplitude there is still some variation, especially in the power, with the structural and material properties. This suggests that an additional bending pattern correction could be introduced into the scaling laws and/or the terms in the current model could be modified to further improve the model's accuracy.

For low thrust and power coefficients, the non-resonating foils follow the scaling law predictions (figures 7(b) and (d)), but they deviate from the predictions at higher coefficients. This is especially clear in the thrust data, and a further analysis of the bending pattern can provide some insight into this deviation. From the motion tracking analysis, the deflection angle of the flexible section relative to the horizontal, β, was measured when the foils' leading section passed through the $\theta = 0$ position (see inset schematic in figure 7(b) for reference). It was discovered that the deflection angle of the flexible section ranged from $0^\circ \lesssim \beta \lesssim 45^\circ$ for the resonating foils and from $0^\circ \lesssim \beta \lesssim 60^\circ$ for the non-resonating foils depending upon the driving frequency. In fact, the data where the deflection angle is $\beta \geqslant 45^\circ$ are

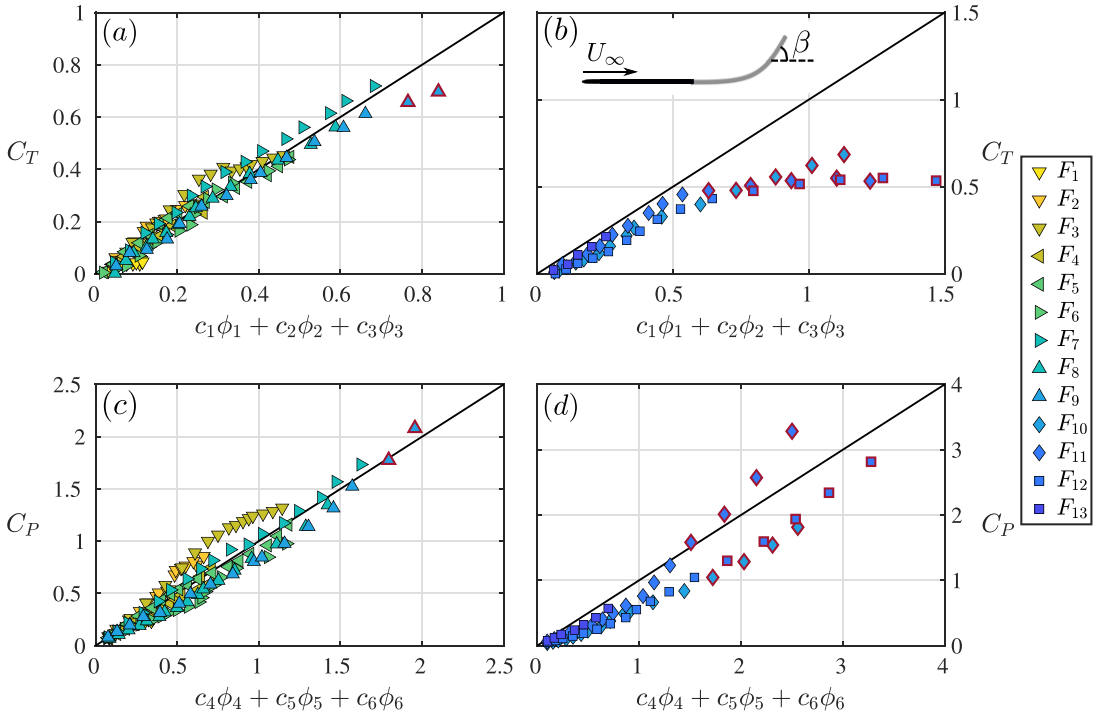

Figure 7. Thrust and power coefficients as functions of the proposed scaling relations developed in [39]. Thrust scaling collapse for (a) the resonating and (b) the non-resonating foils. Power scaling collapse for (c) the resonating and (d) the non-resonating foils. Data are marked by a red outline when the measured deflection angle of the flexible section is $\beta \geqslant 45°$. This angle is measured via motion tracking analysis when the foils pass through the $\theta = 0°$ position as indicated in the inset schematic in (b).

denoted with a red marker outline. It can now be clearly seen that at and above this threshold angle the thrust data deviate from the scaling law. We postulate that at these extreme deflection angles there is flow separation at the flexion point, which in turn leads to additional drag and an over-prediction of the thrust by the scaling law. If confirmed through future flow measurements, an additional term for this phenomenon could be added to the scaling laws to collapse the non-resonating foil data as well.

7. Conclusions

We constructed simple non-uniformly flexible foils with a flexible trailing section joined to a rigid leading section. This produces a basic non-uniform flexibility distribution as a chordwise step function in the flexural rigidity of the foil. Importantly, the flexion ratio and flexural rigidity of the trailing section are varied, which provides, for the first time, a comprehensive experimental examination of the role of the bending pattern in driving the performance of non-uniformly flexible foils operating below, at and above their first natural frequency. The Euler–Bernoulli beam equation is used to derive a novel effective flexibility defined as the ratio of the added mass forces to the elastic forces. This dimensionless variable is a generalization of the effective flexibility derived in Quinn *et al* [14] and it is shown to provide a scaling of the natural frequencies of the fluid-structural system. However, only some of the foils showed a detectable resonance condition at the predicted first natural frequency and were described as 'resonating foils', while the others did not and were described as 'non-resonating foils'. Moreover, motion-tracking software measured the bending pattern of the foils to reveal that the resonating foils exhibited a smooth beam-like deflection while the non-resonating foils exhibited a discontinuous hinge-like deflection.

The thrust and power of the resonating foils showed clear trends with the effective flexibility similar to uniformly flexible foils, while the non-resonating foils showed somewhat similar trends in the thrust, but dramatically different trends in the power, reminiscent of rigid foil data. This led to broad efficiency peaks for the resonating foils and sharper efficiency peaks for the non-resonating foils. Surprisingly, a resonating ($\lambda = 0.4$) and a non-resonating ($\lambda = 0.6$) foil respectively achieved peak efficiencies of 49% and over 50%; equivalent values within the uncertainty of the measurements. These efficiencies are strikingly high for purely pitching three-dimensional foils with $AR = 2$ and amount to a 127% increase in efficiency over the uniformly flexible foil as well as a 150% increase in efficiency over the rigid foil. In fact, it is determined that there is a range of optimal flexion ratios from $0.4 \leqslant \lambda \leqslant 0.7$ that maximizes the efficiency. Also, this coincides with flexion ratios observed in nature [33], which suggests that animals may have evolved bending patterns that enhance their propulsive efficiency. A dimensionless

bending rigidity, R^*, is defined, which incorporates both EI and λ. While the efficiency performance is primarily driven by the resonance condition (Π_k) and the bending pattern (λ), the dimensionless rigidity plays a secondary role in maximizing the efficiency. To achieve high propulsive efficiency non-uniformly flexible hydrofoils should (1) oscillate above their first natural frequency, (2) have a flexion ratio in the range of $0.4 \leqslant \lambda \leqslant 0.7$ and (3) have a small dimensionless rigidity at their optimal flexion ratio.

The amplitude response of non-uniformly flexible foils is found to implicitly capture the overarching effects of flexibility and, when used, it is shown that established scaling laws for pitching foils [39] accurately capture the flow physics. This is true as long as the deflection angle of the flexible section is less than $\beta = 45°$, above which it is suspected that flow separation modifies the flow physics. Future efforts to measure the flow field around these foils, especially at the flexion point, would be beneficial in understanding the connection between flow phenomena, such as separation, and the performance. This would further inform the development of a scaling for the amplitude response of these foils, and more accurate scaling laws that capture the physics of both the resonating and non-resonating foils. Also, future work can investigate how flexibility is interconnected with variations in the planform shape, including the aspect ratio, sweep and curvature of the hydrofoils. Based on [41], we suspect that the kinematics, flexibility and planform shape are intertwined in a way that all three need to be considered simultaneously to determine an optimal design.

Follow-on work has already used a near optimal non-uniformly flexible foil revealed in this study to measure the collective performance of two such foils in a leader–follower arrangement [43]. In that follow-on study it was discovered that with tailored interactions the collective efficiency of two non-uniformly pitching foils could rise to 62% with a near doubling of the thrust coefficient to $C_T = 0.44$; quite an extraordinary performance for purely pitching foils.

Acknowledgments

This work was supported by the Office of Naval Research under Program Director Dr Robert Brizzolara on MURI Grant No. N00014-08-1-0642.

Data availability statement

All data that support the findings of this study are included within the article (and any supplementary files).

ORCID iDs

Tianjun Han https://orcid.org/0000-0002-5319-123X
Amin Mivehchi https://orcid.org/0000-0002-9705-7972
Melike Kurt https://orcid.org/0000-0001-6711-7025

References

[1] Daniel T L 1988 Forward flapping flight from flexible fins *Can. J. Zool.* **66** 630–8
[2] Combes S A and Daniel T L 2001 Shape, flapping and flexion: wing and fin design for forward flight *J. Exp. Biol.* **204** 2073–85
[3] Lauder G V, Madden P G A, Tangorra J L, Anderson E and Baker T V 2011 Bioinspiration from fish for smart material design and function *Smart Mater. Struct.* **20** 094014
[4] Wu T Y-T 1971 Hydromechanics of swimming propulsion: I. Swimming of a two-dimensional flexible plate at variable forward speeds in an inviscid fluid *J. Fluid Mech.* **46** 337–55
[5] Katz J and Weihs D 1978 Hydrodynamic propulsion by large amplitude oscillation of an airfoil with chordwise flexibility *J. Fluid Mech.* **88** 485–97
[6] Prempraneerach P, Hover F S and Triantafyllou M S 2003 The effect of chordwise flexibility on the thrust and efficiency of a flapping foil *Int. Symp. Unmanned Untethered Submersible Technology* available from http//web.mit.edu/arg/www/towtank/papers/FlexibleFoil_Paper.pdf%5Cnpapers3//publication/uuid/2586F91D-B411-406F-9BE7-F472F3577380
[7] Pederzani J and Haj-Hariri H 2006 Numerical analysis of heaving flexible airfoils in a viscous flow *AIAA J.* **44** 2773–9
[8] Masoud H and Alexeev A 2010 Resonance of flexible flapping wings at low Reynolds number *Phys. Rev.* E **81** 056304
[9] Ramananarivo S, Godoy-Diana R and Thiria B 2011 Rather than resonance, flapping wing flyers may play on aerodynamics to improve performance *Proc. Natl Acad. Sci. USA* **108** 5964–9
[10] Kang C-K, Aono H, Cesnik C E S and Shyy W 2011 Effects of flexibility on the aerodynamic performance of flapping wings *J. Fluid Mech.* **689** 32–74
[11] Dai H, Luo H, de Sousa P J S A F and Doyle J F 2012 Thrust performance of a flexible low-aspect-ratio pitching plate *Phys. Fluids* **24** 101903
[12] Hua R N, Zhu L and Lu X-Y 2013 Locomotion of a flapping flexible plate *Phys. Fluids* **25** 121901
[13] Dewey P A, Boschitsch B M, Moored K W, Stone H A and Smits A J 2013 Scaling laws for the thrust production of flexible pitching panels *J. Fluid Mech.* **732** 29–46
[14] Quinn D B, Lauder G V and Smits A J 2014 Scaling the propulsive performance of heaving flexible panels *J. Fluid Mech.* **738** 250–67
[15] Rosic M L N, Thornycroft P J M, Feilich K L, Lucas K N and Lauder G V 2017 Performance variation due to stiffness in a tuna-inspired flexible foil model *Bioinspiration Biomimetics* **12** aa5113
[16] Michelin S and Smith S G L 2009 Resonance and propulsion performance of a heaving flexible wing *Phys. Fluids* **21** 071902
[17] Quinn D B, Lauder G V and Smits A J 2014 Flexible propulsors in ground effect *Bioinspiration Biomimetics* **9** 036008
[18] Quinn D B, Lauder G V and Smits A J 2015 Maximizing the efficiency of a flexible propulsor using experimental optimization *J. Fluid Mech.* **767** 430–48

[19] Paraz F, Schouveiler L and Eloy C 2016 Thrust generation by a heaving flexible foil: resonance, nonlinearities, and optimality *Phys. Fluids* **28** 011903
[20] Goza A, Floryan D and Rowley C 2020 Connections between resonance and nonlinearity in swimming performance of a flexible heaving plate *J. Fluid Mech.* **888** A30
[21] Kancharala A K and Philen M K 2016 Optimal chordwise stiffness profiles of self-propelled flapping fins *Bioinspiration Biomimetics* **11** 056016
[22] Fish F E and Lauder G V 2006 Passive and active flow control by swimming fishes and mammals *Annu. Rev. Fluid Mech.* **38** 193–224
[23] Bose N, Lien J and Ahia J 1990 Measurements of the bodies and flukes of several cetacean species *Proc. R. Soc.* B **242** 163–73
[24] DeBlois M C and Motani R 2019 Flipper bone distribution reveals flexible trailing edge in underwater flying marine tetrapods *J. Morphol.* **280** 908–24
[25] Moore M N J 2015 Torsional spring is the optimal flexibility arrangement for thrust production of a flapping wing *Phys. Fluids* **27** 091701
[26] Floryan D and Rowley C W 2020 Distributed flexibility in inertial swimmers *J. Fluid Mech.* **888** A24
[27] Floryan D and Rowley C W 2018 Clarifying the relationship between efficiency and resonance for flexible inertial swimmers *J. Fluid Mech.* **853** 271–300
[28] Lucas K N, Thornycroft P J M, Gemmell B J, Colin S P, Costello J H and Lauder G V 2015 Effects of non-uniform stiffness on the swimming performance of a passively-flexing, fish-like foil model *Bioinspiration Biomimetics* **10** 056019
[29] Yeh P D, Li Y and Alexeev A 2017 Efficient swimming using flexible fins with tapered thickness *Phys. Rev. Fluids* **2** 102101
[30] Chao L-M, Pan G, Cao Y-H, Zhang D and Yan G-X 2018 On the propulsive performance of a pitching foil with chord-wise flexibility at the high Strouhal number *J. Fluids Struct.* **82** 610–8
[31] Zeyghami S and Moored K W 2019 Effect of nonuniform flexibility on hydrodynamic performance of pitching propulsors *J. Fluids Eng.* **141** 041108
[32] David M J, Govardhan R N and Arakeri J H 2017 Thrust generation from pitching foils with flexible trailing edge flaps *J. Fluid Mech.* **828** 70–103
[33] Lucas K N, Johnson N, Beaulieu W T, Cathcart E, Tirrell G, Colin S P, Gemmell B J, Dabiri J O and Costello J H 2014 Bending rules for animal propulsion *Nat. Commun.* **5** 3293
[34] Weaver W, Timoshenko S P and Young D H 1990 *Vibration Problems in Engineering* 5th edn (New York: Wiley)
[35] Theodore T 1935 *NACA Tech. Rep. 496* Langley Memorial Aeronautical Laboratory General theory of aerodynamic instability and the mechanism of flutter
[36] Garrick I 1936 Propulsion of a flapping and oscillating airfoil *NACA Technical Report 567* Langley Memorial Aeronautical Laboratory
[37] Michelin S and Llewellyn Smith S G 2009 Resonance and propulsion performance of a heaving flexible wing *Phys. Fluids* **21** 071902
[38] Das A, Shukla R K and Govardhan R N 2016 Existence of a sharp transition in the peak propulsive efficiency of a low-pitching foil *J. Fluid Mech.* **800** 307–26
[39] Moored K W and Quinn D B 2017 Inviscid scaling laws of a self-propelled pitching airfoil *AIAA J.* **57** 3686–700
[40] Akoz E and Moored K W 2017 Unsteady propulsion by an intermittent swimming gait *J. Fluid Mech.* **834** 149–72
[41] Ayancik F, Zhong Q, Quinn D B, Brandes A, Bart-Smith H and Moored K W 2018 Scaling laws for the propulsive performance of three-dimensional pitching propulsors *J. Fluid Mech.* **871** 1117–38
[42] Mivehchi A, Zhong Q, Kurt M, Quinn D B and Moored K W 2021 Scaling laws for the propulsive performance of a purely pitching foil in ground effect *J. Fluid Mech.* **919** R1
[43] Kurt M, Mivehchi A and Moored K 2021 High-efficiency can be achieved for non-uniformly flexible pitching hydrofoils via tailored collective interactions *Fluids* **6** 10–4